Catalysis Science & Technology

Accepted Manuscript

ROYAL SOCIETY OF CHEMISTRY

www.rsc.org/catalysis

Graphical abstract

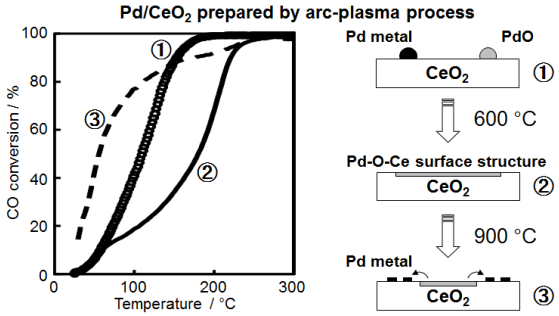

High CO oxidation activity of Pd/CeO_2 as prepared by using arc-plasma process was lost by thermal ageing at 600 °C in air, whereas further ageing at 900 °C enhanced significantly the activity, exceeding that of the as-prepared catalyst, because of the highly dispersed metallic Pd nanoparticles formed by thermal dissociation of Pd-O-Ce surface moieties.

Effect of thermal ageing on the structure and catalytic activity of Pd/CeO_2 prepared using arc-plasma process

Satoshi Hinokuma[1, 2], Hiroaki Fujii[1], Yasuo Katsuhara[1],

Keita Ikeue[1,2], Masato Machida[1,2] *

[1]*Department of Applied Chemistry and Biochemistry,*

Graduate School of Science and Technology, Kumamoto University,

2-39-1 Kurokami, Chuo, Kumamoto, 860-8555 Japan

[2]*Unit of Elements Strategy Initiative for Catalysts & Batteries, Center for The Promotion of Interdisciplinary Education and Research, Kyoto University*

Kyoto Daigaku Katsura, Saikyo-ku, Kyoto, 615-8520 Japan

CORRESPONDING AUTHOR:

Prof. Masato Machida

Department of Applied Chemistry and Biochemistry,

Graduate School of Science and Technology,

Kumamoto University,

2-39-1 Kurokami, Chuo, Kumamoto, 860-8555 Japan

TEL/FAX:+81-96-342-3651

E-mail: machida@kumamoto-u.ac.jp

Abstract

Pd nanoparticles were deposited onto CeO_2 powders using an arc-plasma process in order to study their thermal behaviour and catalytic activity for CO oxidation. As-prepared catalyst exhibited a higher catalytic activity than catalysts prepared *via* conventional wet-impregnation because the metallic state of Pd responsible for CO oxidation activity is abundant. The activity was decreased by thermal ageing at 600 °C in air, which oxidized metallic Pd to the oxide interacting with the surface of CeO_2. On the other hand, ageing at 900 °C in 10% H_2O/air significantly enhanced the activity, regardless of sintering of CeO_2, to show the highest activity, as observed in our previous work for the catalyst prepared by conventional wet-impregnation. The activation by thermal ageing is associated with the thermodynamic dissociation of the oxidic Pd to metallic Pd species at 900 °C.

Keywords: Arc-plasma process, Pd, CeO_2, Metal-support interaction, CO oxidation

Introduction

Pd catalysts supported on CeO_2 have attracted considerable attention because the interactions at the metal/support interface allow synergistic oxidation/reduction of both components.[1-3] Many researchers have been interested in low-temperature CO oxidation over Pd/CeO_2 because the catalytic activity is sensitive to the particle size and the oxidation state of Pd, oxygen deficiency of CeO_2 surface and/or other structural features of the metal-support interface.[4-19] As a consequence, catalyst preparation and pretreatment are crucial issues. Fernández-García et al.[4] reported the room-temperature CO oxidation activity of $Pd/CeO_2/\gamma\text{-}Al_2O_3$ prepared *via* wet-impregnation and concluded that CeO_2 promotes the formation of metallic Pd species efficient for CO activation and oxygen vacancies enabling O_2 activation on the Pd-CeO_2 interfacial site. The CO oxidation at room-temperature over Pd/CeO_2 was also reported by Boronin et al.[6] who found highly dispersed Pd formed as a surface interaction phase ($Pd_xCeO_{2-\delta}$) and subnano-particle Pd metal. More recently, Colussi et al.[19] reported the formation of a Pd-O-Ce surface superstructure in Pd/CeO_2 as revealed by DFT calculations based on high-resolution TEM observations.

We reported that thermal ageing at 900 °C improves the catalytic activity of Pd/CeO_2 for low-temperature CO oxidation in spite of significant sintering of the CeO_2 support.[20] Strong metal-support interaction via Pd-O-Ce bonding on the surface prevent the sintering of Pd oxide at ≤800 °C but are converted to active metallic Pd nanoparticles at ~900 °C, at which point the equilibrium PdO/Pd phase transformation is reached. The metallic Pd nanoparticles intimately contacting CeO_2 are believed to be responsible for CO adsorption and the subsequent reactions with oxygen near room temperature.

In the present work, we focused on the preparation of Pd/CeO_2 using a pulsed arc-plasma technique and the effect of thermal ageing on the as-prepared catalyst. As was

reported in our recent papers,[21-24] the arc-plasma catalyst preparation method enables the one-step deposition of metal nanoparticles from bulk metals onto various support powders. The as-prepared catalysts are characterized by highly dispersed and uniform metallic nanoparticles and thus are characterized by high catalytic activity. However, it should be noted some of these catalysts are readily deactivated by thermal ageing due to weaker metal-support interactions compared to those of catalysts prepared *via* wet-impregnation processes.[22, 23] In this regard, Pd/CeO_2 with its strong intrinsic metal-support interactions is the most interesting candidate to apply arc-plasma catalyst preparation. The structures and catalytic properties of as-prepared and thermally-aged Pd/CeO_2 catalysts were studied using XPS, XAFS and chemisorption analyses. The results were compared to those obtained for reference catalysts prepared using a conventional wet-impregnation method, which were studied previously.[20]

Experimental

Catalyst preparation

Pd/CeO_2 catalyst powders were prepared using a pulsed cathodic arc-plasma process as previously reported.[21-24] High purity CeO_2 (Rhodia, 99.99%) was used after heating at 200 °C in vacuo (Table S1 and Fig. S1 in ESI for physicochemical properties of CeO_2). The catalyst preparation apparatus consisted of a vacuum chamber with a turbo-molecular pumping system, an arc-plasma gun (Ulvac Inc., ARL-300) with a Pd cathode (ϕ10 mm, Furuya Metals, Co. Ltd.), and a powder container with a rotating stirring mechanism. Prior to deposition of the Pd nanoparticles, the vacuum chamber was filled with N_2 and evacuated below 1×10^{-3} Pa overnight in order to remove any gases adsorbed on the CeO_2. A quadrupole mass spectrometer was used to analyze the residual gas, which consisted mainly of N_2 and H_2O. A

pulsed arc-plasma with a period of 0.2 ms and current amplitude of 2 kA was generated with a frequency of 2 Hz. Pd particle size and deposition rate can be controlled by the input energy, which is expressed by $E = (1/2)CV^2$, where C is electric capacitor and V is applied discharge voltage. Based on the preliminary study on the effect of E on the size of as-deposited nanoparticles using a Rh cathode (Fig. S2 in ESI for size distribution of as-deposited metal nanoparticles), the present study was performed using the following parameters: C = 360 μF, V = 125 V and E = 3 J. The plasma thus generated from the Pd cathode entered into the container filled with CeO_2 powders (BET surface area: 173 $m^2 \cdot g^{-1}$) with stirring at a rotation rate at 60 rpm. The pressure was maintained at less than 1×10^{-3} Pa during the deposition. The amount of Pd loading after 20000 pulses was approximately 0.4 wt%. A catalyst with the same composition was also prepared *via* a conventional wet-impregnation method using an aqueous solution of $Pd(NO_3)_2$ and subsequently heated at 600 °C for 3 h in air, as was reported in our previous study.[20] The catalysts prepared *via* the arc-plasma process and wet-impregnation method are denoted as 'AP' and 'imp', respectively. The as-prepared catalysts were both thermally aged in the following sequence: (i) 600 °C for 3 h in air, (ii) 900 °C for 25 h in 10% H_2O/air and (iii) 600 °C for 25 h in dry air. The catalysts after each thermal ageing step are denoted in Table 1.

Characterization

X-ray diffraction (XRD) analysis was performed using monochromated Cu K_α radiation (30 kV, 30 mA, Rigaku Multiflex). The loading of Pd was determined using X-ray fluorescence analysis (Rigaku EDXL300). High-resolution TEM (HRTEM) observations were carried out using an FEI TECNAI F20 electron microscope operating at 200 kV. The BET surface areas (S_{BET}) were calculated from N_2 adsorption isotherms obtained at 77 K

(Belsorp-mini, BEL Japan, Inc.). The metal dispersion of Pd metal was determined after H_2 reduction treatment at 200 °C using the modified pulsed CO technique (BELCAT-B, BEL Japan, Inc.) developed by Takeguchi et al.[25], which uses the preinjection of CO_2 to prevent overestimation caused by CO adsorption onto CeO_2 as carbonate species. The metal dispersion was expressed in terms of CO/Pd, the molar ratio of CO chemisorbed to Pd loaded on the CeO_2. Because *in situ* FT-IR spectra suggested that CO chemisorbed on catalyst AP1 in both linear (CO:Pd = 1:1) and bridged (1:2) forms, the average stoichiometry was estimated from the peak areas of each absorbed species to be CO:Pd = 1:1.6 (Fig. S3 in the ESI for the determination of CO adsorption stoichiometry). This value was used to calculate the mean particle size of Pd as deposited on CeO_2.

XPS spectra were obtained on a VG Sigmaprobe spectrometer using Mg Kα radiation (15 kV, 20 mA). The chemical shifts in the XPS spectra were calibrated using the binding energy of the C1s XPS spectrum at 285.0 eV. The intensity of the C1s peak of the Pd/CeO_2 catalyst as prepared using the AP process was nearly the same as that of neat CeO_2, suggesting that no measurable carbon deposition occurred during the arc-plasma catalyst preparation. The X-ray absorption spectra of Pd at the K-edge were obtained using the NW10A station at the Photon Factory for Advanced Ring (PF-AR), High Energy Accelerator Research Organization (KEK) at Tsukuba (Proposal No. 2012G749). The XPS and XAFS analyses were performed without any pretreatment of the catalysts.

Catalytic reactions

Catalytic CO oxidation was performed in a flow reactor at atmospheric pressure. The as-prepared catalyst (10–20 mesh, 50 mg) was fixed in a quartz tube (ϕ6 mm) with quartz wool at both ends of the catalyst bed. The temperature dependence of the catalytic activity

was evaluated by heating the catalyst bed from room temperature to 600 °C at a constant rate of 10 °C·min^{-1}, while supplying a gas mixture containing CO (0.1%), O_2 (1.25%) and He (balance) at 100 cm^3·min^{-1} (W/F = 5.0 × 10^{-4} g·min·cm^{-3}). The concentration of CO and CO_2 in the effluent gas was analysed using a Horiba VA3000 NDIR gas analyzer.

Results and Discussion

Microstructure of Pd/CeO_2 prepared using the AP process

Figure 1a shows a TEM image and the size distribution of Pd nanoparticles as directly deposited onto a TEM grid covered with a microgrid carbon film. Highly dispersed nanoparticles with an average diameter of 2.4 ± 0.8 nm were observed. The histogram analysis clearly suggested a very narrow size distribution ranging from 1 nm to 5 nm. The HRTEM image shown in Figure 1b suggests that the nanoparticles were crystalline, with the lattice spacing of 0.22 nm interpreted to be the d_{110} of PdO. In addition, the FFT pattern of the nanoparticle in Figure 1c corresponds to a diffraction pattern taken along the [111] zone axis showing $(1\,\bar{1}\,0)$ and $(0\,\bar{1}\,1)$ spots, confirming that these nanoparticles were crystallized PdO. On the other hand, Pd nanoparticles containing metallic Pd with the face-centred cubic structure were also observed in the TEM image and FFT pattern. The size and morphology of the present system are similar to that of Rh and Pt nanoparticles previously prepared under the same conditions.[22, 23]

The XRD pattern of the as-prepared Pd/CeO_2 catalyst showed peaks ascribable to CeO_2 with a cubic fluorite-type structure, which became intense and sharp after thermal ageing at 900 °C due to sintering. However, the diffraction peaks for Pd and its oxide could not be observed due to the low loading level (Fig. S4 in ESI for XRD patterns). The microstructure of the Pd/CeO_2 as prepared using the arc-plasma process was also observed via

TEM. Figure 2 shows TEM images of Pd/CeO_2 before (AP1) and after ageing at 900 °C in 10% H_2O/air (AP3). In AP1, small grains of CeO_2 with a diameter of a few nanometers were observed. By contrast, AP3 consisted of much larger grains of CeO_2 (>100 nm) exhibiting a neck growth as a consequence of sintering. In both images, it is difficult to discriminate the Pd/PdO nanoparticles from the background CeO_2 particles with a high contrast, as was previously the case for Pd/CeO_2(imp).[20] The particle size of the Pd deposited onto CeO_2 was thus estimated based on CO chemisorption to be 1.7 nm. This result is in accordance with the TEM results in Fig. 1a, suggesting that the Pd nanoparticles deposited on the surface of CeO_2 were similar to those deposited on the TEM microgrid. In addition, this observation is in agreement with the behaviour of Pt and/or Rh deposited under the same arc-plasma process conditions,[22, 23] which had particle sizes of approximately 2~3 nm regardless of the type of support material (Al_2O_3, $AlPO_4$, etc.).

Effect of thermal ageing on CO oxidation activity

Figure 3a shows the temperature dependences of CO conversion over Pd/CeO_2 as prepared using the arc-plasma process and after stepwise thermal ageing. The effect of thermal ageing can be observed from the shift of these so-called light-off curves. The as-prepared Pd/CeO_2 (AP1) catalyst initiated the reaction at a low temperature of approximately 25 °C, whereas ageing at 600 °C (AP2) caused the shift of the light-off temperature to higher values. Interestingly, however, light-off near ambient temperature was restored by further ageing at 900 °C (AP3), and was not affected by subsequent ageing at 600 °C (AP4). When the catalyst was prepared *via* wet-impregnation and subsequent calcination at 600 °C (imp2), the activity was very low (Figure 3b). In accordance with our previous study,[20] however, ageing at 900 °C enhanced the activity, and this increased activity was not lost upon further ageing at 600 °C.

The observation of this similar trend for the AP and imp catalysts during thermal ageing suggested that the Pd/CeO_2 prepared using both methods obeyed the same activation/deactivation mechanism.

To understand the complicated thermal behaviour of the Pd/CeO_2 catalysts, the BET surface area (S_{BET}), metal dispersion (CO/Pd), Pd oxidation state, light-off temperature for CO oxidation (T_{50}) and turnover frequency (TOF) were determined for each and are compared in Table 1. Stepwise thermal ageing decreased the S_{BET} of the as-prepared Pd/CeO_2 (AP1) catalyst from 162 $m^2 \cdot g^{-1}$ (AP1) to 107 $m^2 \cdot g^{-1}$ (600 °C, AP2) and then to approximately 10 $m^2 \cdot g^{-1}$ (900 °C, AP3/AP4). Similar sintering behaviour was observed for the catalyst prepared *via* wet-impregnation (imp2-4). In complete contrast to the loss of S_{BET}, however, a noticeable increase in the CO/Pd values occurred with an increase in the ageing temperature from 42% (AP1) to 51% (600 °C, AP2) and then to greater than 90% (900 °C, AP3/AP4). It should be noted that the extremely high values observed after ageing at 900 °C are indicative of an overestimation of the amount of CO chemisorption due to spillover of CO and adsorption onto CeO_2 as CO_2. Although CO_2 pre-adsorption was applied in order to minimize this effect, it was difficult to completely eliminate it for the Pd/CeO_2 catalyst thermally aged at high temperature.

The oxidation state of Pd was determined using XPS. Figure 4 shows the Pd3d and Ce3d XPS spectra, the intensity of which is normalized to the intensity of the Ce3d line. The Pd3d XPS spectra exhibited two sets of spin orbital doublets for $Pd3d_{5/2}$ and $Pd3d_{3/2}$ assignable to Pd^0 and Pd^{2+}. The as-prepared Pd/CeO_2 (AP1) catalyst contained 41% Pd in the metallic state (Pd^0). Basically, the AP process under vacuum yields metallic nanoparticles, but a certain portion is oxidized when exposed to air. Although thermal ageing at 600 °C completely converted Pd^0 to oxidized Pd^{2+}, further ageing in 10% H_2O/air at 900 °C reduced

more than 70% of the Pd to the metallic state, which remained nearly unchanged during subsequent ageing at 600 °C. As revealed in our previous study,[20] the impregnated catalyst, Pd/CeO_2(imp2), exhibited a similar change in the Pd oxidation state. The binding energy of Pd^{2+} observed in each catalyst after heating at 600 °C was approximately 337.5 eV. These values are higher than those reported for bulk PdO (336.80 eV) and close to those of $PdCl_2$ and $Pd(NO_3)_2$.[26, 27] Priolkar et al. also reported a higher shift for the Pd^{2+} XPS signals of their solution combustion-synthesized Pd/CeO_2, which contains Pd-O-Ce bonding in a pseudo solid solution phase.[28] They proposed Pd^{2+} in a higher ionic state is stabilized in Ce^{3+} sites, leading to strong Pd-O-Ce bonding interactions. We believe that a similar interaction between Pd oxide and CeO_2 occurred in the present system, as discussed in the next section.

It should also be noted that the Pd3d peak for AP1 was less intense than the corresponding peaks after thermal ageing. The normalized Pd3d peak intensity is related to the Pd surface coverage (Pd/Ce) and photoelectron escape depth. In the uncalcined catalyst (AP1), a large number of Pd is inside the pores, and the photoelectrons from these Pd atoms cannot escape due to absorption by the CeO_2 matrix. By contrast, Pd is mainly located on the exterior of the low-surface area CeO_2 after thermal ageing at 900 °C. The observed change in the peak intensity is thus associated with the grain growth of CeO_2 during thermal ageing. The peak deconvolution of the Ce3d XPS spectra (Figure 4c) yielded two sets of peaks, which were assigned to Ce^{3+} (V^0, V', U^0, and U' shown as red lines) and Ce^{4+} (V, V'', V''', U, U'', and U''' shown as black lines) as have been reported by several researchers.[6, 11, 29] The surface concentration ratio (Ce^{3+}/Ce^{4+}) of the CeO_2 was in the range of 32–38%, which was the same as that for the neat CeO_2 (Fig. S1 in ESI). The surface properties of CeO_2 were thus not affected by loading the small amount of Pd (0.4 wt%) used in the present system.

Table 1 also indicates the catalytic activity in terms of the T_{50}, which is the temperature for 50% CO conversion, and the TOF, which was calculated using the rate of CO conversion at 50 °C and the Pd dispersion level (CO/Pd). The values for T_{50} suggest that the apparent activity decreased upon ageing at 600 °C and then increased after further heating at 900 °C, in accordance with the level of Pd dispersion (CO/Pd) and/or fraction of metallic Pd species. However, because a similar trend was observed for TOF values, the activity per unit Pd site should be closely associated with the Pd oxidation state.

Local structure of Pd/CeO_2 prepared using the AP process

Figure 5 shows Fourier transforms of the Pd K-edge EXAFS for the Pd/CeO_2 as prepared using the arc-plasma process (AP1) and after thermal ageing (AP2 and AP3), together with those of the impregnated catalysts (imp2 and imp3) and two references (Pd and PdO). The observed peaks are shifted to shorter *r*-values from true atomic distances because these spectra are not corrected for phase shifts. The best curve-fitting is obtained when the first and second coordination shells are filtered, and the resultant structural parameters, including the phase shift corrected *r*-values, are listed in Table 2. The as-prepared Pd/CeO_2 (AP1) catalyst exhibited an intense peak assignable to a Pd-O (r = 1.97 Å) shell, but the second coordination contained contributions from Pd to Pd (r = 2.74 Å) and Pd-O-Ce (r = 3.14 Å) shells. This result is in accordance with the XPS results (Table 1), suggesting the coexistence of metallic and oxidic Pd species. After ageing at 600 °C (AP2), the Pd-Pd shell was lost with the simultaneous appearance of a Pd-O-Pd shell, but the intensified Pd-O-Ce shell suggested the formation of PdO/CeO_2 interface bonds. As Colussi et al.[19] revealed using density-functional theory (DFT) calculations based on high-resolution TEM images, the formation of a Pd-O-Ce surface superstructure consisting of a square-planar PdO_4 unit, the Pd of which is coordinated

by two O atoms of the top layer of the CeO_2 (110) surface and by two O atoms of the second layer, is possible. The structural model is in accordance with our recent analysis using EXAFS/XPS of Pd/CeO_2 prepared *via* conventional wet impregnation and subsequent calcination at a moderate temperature (~600 °C).[20] We have proposed that such a Pd-O-Ce surface moiety plays a key role in the prevention of the sintering of Pd oxide species up to 800 °C and the formation of highly dispersed metallic Pd species when calcination occurs at ≥800 °C. This behaviour is also apparent for the present Pd/CeO_2 catalyst prepared using an AP process; thermal ageing at 900 °C (AP3) yielded the Pd-Pd shell and was accompanied by increased Pd dispersion (Table 1). Although the EXAFS results of the present impregnated catalyst, imp2, also indicate the presence of these interactions, the obtained coordination numbers for Pd-O-Ce (*CN* = 4.1) are slightly different from those for AP2 (*CN* = 1.9), suggesting that the Pd-O-Ce bonding in AP2 is weaker than that in imp2.

Possible mechanisms for the effect of thermal ageing

The effect of thermal ageing on the catalytic activity of Pd/CeO_2 prepared using an AP process was then considered. As is evident from Table 1, a high BET surface area is not essential for an active catalyst, but Pd dispersion and its oxidation state are rather important. Higher Pd dispersion is desired and metallic Pd is more active than Pd oxide (PdO) for CO oxidation.[6] A possible mechanism that explains the thermal behaviour of the present system is illustrated in Figure 6. In the as-prepared catalyst fabricated using AP (AP1), nanoparticles of Pd metal were highly dispersed on the CeO_2. A portion of these nanoparticles was oxidized upon exposure to air and oxidation was complete after heating at 600 °C (AP2). The lowest activity after ageing at 600 °C resulted because the Pd was in the form of the oxide, unlike in the as-prepared (AP1) catalyst, and the catalyst aged at 900 °C (AP3), which contained

metallic Pd. A portion of these oxidized Pd species in AP2 formed Pd-O-Ce bonds on the surface of the CeO_2, which prevented the sintering of the Pd oxide species. When the thermodynamic equilibrium between the Pd oxide species and Pd metal was reached at 900 °C (AP3), the dissociation of the Pd oxide species yielded a number of metallic Pd nanoparticles with high dispersion. Therefore, AP3 exhibited the highest activity, even after significant sintering of the CeO_2. Because the metallic Pd nanoparticles deposited on the CeO_2 were then stabilized and resistant to reoxidation at 600 °C, the high catalytic activity was retained, even after subsequent ageing at 600 °C (AP4). Interestingly, this result was not observed for a previously studied Pt/CeO_2 catalyst,[23] the Pt dispersion of which was substantially decreased due to the sintering of the CeO_2 upon thermal ageing at 900 °C. The Pt/CeO_2 catalyst prepared using the AP process was therefore deactivated to a larger extent than the corresponding impregnated catalyst. It can thus be concluded that the tolerance against sintering by means of anchoring to CeO_2 is more efficient for Pd than Pt. Pd is stable in the form of oxide species at 600 °C, which are able to form Pd-O-Ce bonds at the interface. By contrast, Pt is in the metallic state at 600 °C and its interactions with CeO_2 are therefore expected to be much weaker.

Conclusions

Metallic Pd nanoparticles of approximately 2 nm in size were deposited on CeO_2 powders using a pulsed arc-plasma process under a vacuum. The as-prepared Pd/CeO_2 catalyst exhibited high catalytic activity for CO oxidation, whereas thermal ageing in air caused complicated changes in the catalytic activity. Ageing at 600 °C converted the Pd into oxide (Pd^{2+}) species, a portion of which interacted strongly with the CeO_2 to form Pd-O-Ce surface bonds. These interactions played a key role in maintaining the high dispersion of the Pd on

the surface of the CeO_2, although the Pd oxide species were much less active for CO oxidation than metallic Pd. Further ageing at 900 °C significantly enhanced the CO oxidation activity because the PdO/Pd phase equilibration caused the thermodynamic dissociation of the Pd oxide species to yield a number of metallic Pd nanoparticles capable of activating CO. The metallic Pd thus formed was stable and its reoxidation during subsequent ageing at 600 °C was very slow.

Acknowledgements

This study was supported by the 'Elements Science and Technology Project' of MEXT Japan and partially supported by the MEXT program 'Elements Strategy Initiative to Form Core Research Centers'. The XAFS experiments were carried out on the NW10A at the Photon Factory (PF), High Energy Accelerator Research Organization (KEK) (Proposal No. 2012G749).

References

1. A. Trovarelli, *Catalysis by ceria and related materials*, Imperial College Press, London, 2002.
2. R. Farrauto and R. Heck, *Catalysis Today*, 1999, **51**, 351-360.
3. J. Kaspar, P. Fornasiero and M. Graziani, *Catalysis Today*, 1999, **50**, 285-298.
4. M. Fernandez-Garcia, A. Martinez-Arias, L. Salamanca, J. Coronado, J. Anderson, J. Conesa and J. Soria, *Journal of Catalysis*, 1999, **187**, 474-485.
5. M. Fernandez-Garcia, A. Martinez-Arias, A. Iglesias-Juez, A. B. Hungria, J. A. Anderson, J. C. Conesa and J. Soria, *Applied Catalysis B-Environmental*, 2001, **31**, 39-50.
6. A. Boronin, E. Slavinskaya, I. Danilova, R. Gulyaev, Y. Amosov, P. Kumetsov, I. Polukhina, S. Koscheev, V. Zaikovskii and A. Noskov, *Catalysis Today*, 2009, **144**, 201-211.
7. E. M. Slavinskaya, R. V. Gulyaev, O. A. Stonkus, A. V. Zadesenets, P. E. Plyusnin, Y. V. Shubin, S. V. Korenev, A. S. Ivanova, V. I. Zaikovskii, I. G. Danilova and A. I. Boronin, *Kinetics and Catalysis*, 2011, **52**, 282-295.
8. R. Gulyaev, A. Stadnichenko, E. Slavinskaya, A. Ivanova, S. Koscheev and A. Boronin, *Applied Catalysis a-General*, 2012, **439**, 41-50.
9. E. Bekyarova, P. Fornasiero, J. Kaspar and M. Graziani, *Catalysis Today*, 1998, **45**, 179-183.
10. O. Pozdnyakova, D. Teschner, A. Wootsch, J. Krohnert, B. Steinhauer, H. Sauer, L. Toth, F. Jentoft, A. Knop-Gericke, Z. Paal and R. Schlogl, *Journal of Catalysis*, 2006, **237**, 17-28.
11. E. L. Wilson, Q. Chen, W. A. Brown and G. Thornton, *Journal of Physical Chemistry*

C, 2007, **111**, 14215-14222.

12. H. Zhu, Z. Qin, W. Shan, W. Shen and J. Wang, *Journal of Catalysis*, 2004, **225**, 267-277.
13. A. Bourane and D. Bianchi, *Journal of Catalysis*, 2004, **222**, 499-510.
14. M. Bowker, I. Jones, R. Bennett, F. Esch, A. Baraldi, S. Lizzit and G. Comelli, *Catalysis Letters*, 1998, **51**, 187-190.
15. S. Oh and G. Hoflund, *Journal of Physical Chemistry a*, 2006, **110**, 7609-7613.
16. S. Oh and G. Hoflund, *Journal of Catalysis*, 2007, **245**, 35-44.
17. S. Penner, P. Bera, S. Pedersen, L. Ngo, J. Harris and C. Campbell, *Journal of Physical Chemistry B*, 2006, **110**, 24577-24584.
18. L. Meng, A. P. Jia, J. Q. Lu, L. F. Luo, W. X. Huang and M. F. Luo, *Journal of Physical Chemistry C*, 2011, **115**, 19789-19796.
19. S. Colussi, A. Gayen, M. Camellone, M. Boaro, J. Llorca, S. Fabris and A. Trovarelli, *Angewandte Chemie-International Edition*, 2009, **48**, 8481-8484.
20. S. Hinokuma, H. Fujii, M. Okamoto, K. Ikeue and M. Machida, *Chemistry of Materials*, 2010, **22**, 6183-6190.
21. S. Hinokuma, K. Murakami, K. Uemura, M. Matsuda, K. Ikeue, N. Tsukahara and M. Machida, *Topics in Catalysis*, 2009, **52**, 2108-2111.
22. S. Hinokuma, M. Okamoto, E. Ando, K. Ikeue and M. Machida, *Catalysis Today*, 2011, **175**, 593-597.
23. S. Hinokuma, M. Okamoto, E. Ando, K. Ikeue and M. Machida, *Bulletin of the Chemical Society of Japan*, 2012, **85**, 144-149.
24. S. Hinokuma, Y. Katsuhara, E. Ando, K. Ikeue and M. Machida, *Catalysis Today*, 2013, **201**, 92-97.

25. T. Takeguchi, S. Manabe, R. Kikuchi, K. Eguchi, T. Kanazawa, S. Matsumoto and W. Ueda, *Applied Catalysis a-General*, 2005, **293**, 91-96.

26. M. Brun, A. Berthet and J. Bertolini, *Journal of Electron Spectroscopy and Related Phenomena*, 1999, **104**, 55-60.

27. T. Pillo, R. Zimmermann, P. Steiner and S. Hufner, *Journal of Physics-Condensed Matter*, 1997, **9**, 3987-3999.

28. K. Priolkar, P. Bera, P. Sarode, M. Hegde, S. Emura, R. Kumashiro and N. Lalla, *Chemistry of Materials*, 2002, **14**, 2120-2128.

29. R. V. Gulyaev, E. M. Slavinskaya, S. A. Novopashin, D. V. Smovzh, A. V. Zaikovskii, D. Y. Osadchii, O. A. Bulavchenko, S. V. Korenev and A. I. Boronin, *Applied Catalysis B: Environmental*, 2014, **147**, 132-143.

Table 1 BET Surface area (S_{BET}), Pd metal dispersion (CO/Pd), amount of Pd^0, catalytic activity (T_{50}) and turnover frequency (TOF) for Pd/CeO_2 catalysts before and after thermal ageing

entry	thermal ageing	S_{BET} / $m^2 \cdot g^{-1}$	CO/Pd [a] / %	Pd^0 / $(Pd^{2+} + Pd^0)$ [b]	T_{50} [c] / °C	TOF [d] / 10^{-2} s^{-1}
AP1	none	162	42	41	109	0.60
AP2	AP1 + 600 °C × 3 h [e]	107	51	0	179	0.51
AP3	AP2 + 900 °C × 25 h [f]	11	94	74	55	1.8
AP4	AP3 + 600 °C × 25 h [g]	15	100	86	62	1.5
imp2	600 °C × 3 h [e]	116	58	0	300	0.12
imp3	imp2 + 900 °C × 25 h [f]	11	74	71	71	2.2
imp4	imp3 + 600 °C × 25 h [g]	12	73	86	86	1.8

[a] Molar ratio of CO chemisorbed to Pd loaded on CeO_2 at 50 °C.

[b] Determined from the Pd3d XPS spectra (Figure 4a and b).

[c] Temperature at which CO conversion reached 50%.

[d] Turnover frequency calculated from the CO conversion at 50 °C.

[e] 600 °C × 3 h in dry air.

[f] AP2/imp2 + 900 °C × 25 h in 10 vol% H_2O/air.

[g] AP3/imp3 + 600 °C × 25 h in dry air.

Table 2 Fitting parameters obtained from analysis of the Pd K-edge EXAFS for the Pd/CeO_2 catalysts

entry	thermal ageing	shell	*CN* [a] (±0.2)	*r* / Å [b] (±0.03)	σ^2 / 10^{-2} Å^2 [c] (±0.05)
AP1	none	Pd-O	2.7	1.97	0.48
		Pd-Pd	0.65	2.74	0.61
		Pd-O-Ce	1.2	3.14	0.64
AP2	AP1 + 600 °C × 3 h [d]	Pd-O	4.1	1.98	0.48
		Pd-O-Pd	0.67	3.04	0.58
		Pd-O-Ce	1.9	3.17	0.61
AP3	AP2 + 900 °C × 25 h [e]	Pd-O	2.9	1.98	0.48
		Pd-Pd	0.70	2.75	0.61
		Pd-O-Ce	1.9	3.14	0.61
imp2	600 °C × 3 h [d]	Pd-O	4.2	2.00	0.48
		Pd-O-Ce	4.1	3.15	0.61
imp3	imp2 + 900 °C × 25 h [e]	Pd-O	4.1	1.99	0.48
		Pd-Pd	0.72	2.75	0.61
		Pd-O-Ce	2.2	3.15	0.61
Pd foil		Pd-Pd	12.0	2.75	0.61
PdO		Pd-O	4.0	2.02	0.48
		Pd-O-Pd	4.0	3.04	0.58
		Pd-O-Pd	8.0	3.42	0.67

Interval from the *k*-space to the *r*-space for FT is 3.0–16.0 Å^{-1}.

[a] Coordination number.

[b] Interatomic distance.

[c] Debye–Waller factor.

[d] 600 °C × 3 h in dry air

[e] AP2/imp2 + 900 °C × 25 h in 10 vol% H_2O/air.

Figure captions

Figure 1 (a) TEM image and size distribution, (b) high-resolution structure image and (c) FFT pattern of unsupported Pd nanoparticles deposited using arc-plasma process.

Figure 2 TEM images of Pd/CeO_2 before (AP1) and after ageing at 900 ℃ for 25 h in a flow of 10% H_2O/air (AP3).

Figure 3 Temperature dependence of CO oxidation over (a) Pd/CeO_2(AP1~AP4) and (b) Pd/CeO_2(imp2~imp4) before and after thermal ageing. Reaction conditions: 0.1% CO, 1.25% O_2, He balance, W/F = 5.0×10^{-4} g·min·cm^{-3}.

Figure 4 Pd3d XPS spectra of (a) Pd/CeO_2 (AP1~AP4) and (b) Pd/CeO_2 (imp2~imp4) and (c) Ce3d XPS spectra of Pd/CeO_2 (AP1, AP3, imp2 and imp3).

Figure 5 Fourier transforms of k^3-weighted Pd K-edge EXAFS for Pd/CeO_2(AP1~AP3) and Pd/CeO_2(imp2 and imp3) and references (PdO and Pd foil).

Figure 6 Possible structural changes in Pd/CeO_2(AP1~AP4) during thermal ageing.

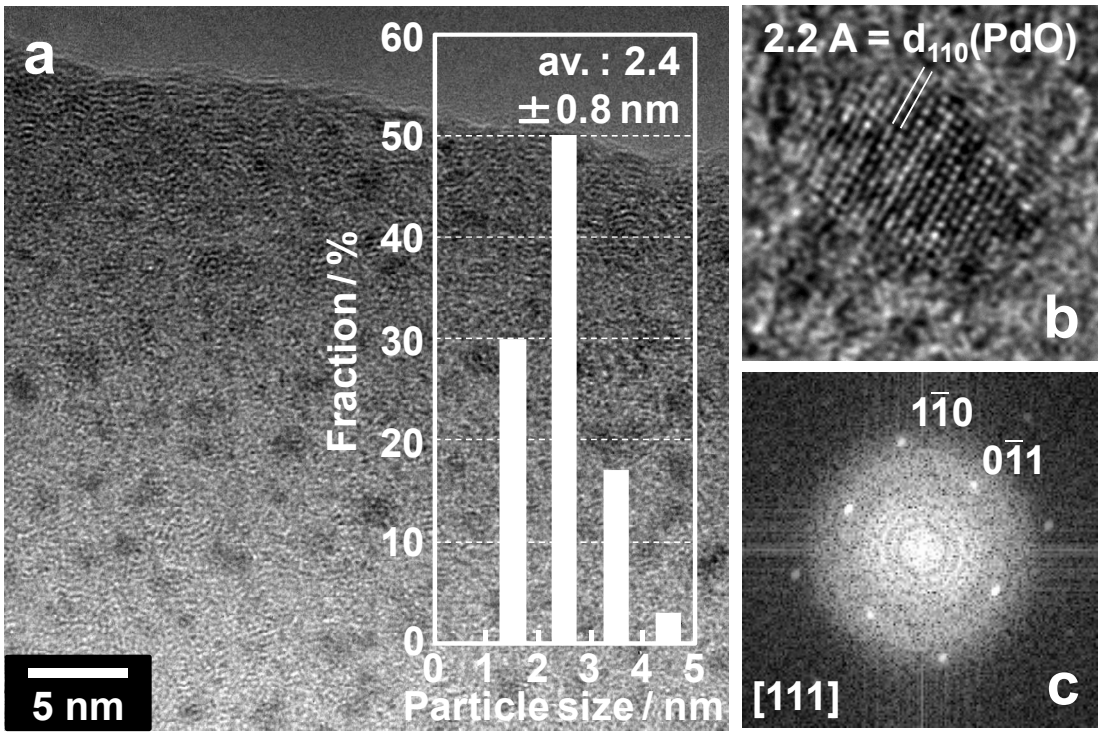

Figure 1 (a) TEM image and size distribution, (b) high-resolution structure image and (c) FFT pattern of unsupported Pd nanoparticles deposited using an arc-plasma process.

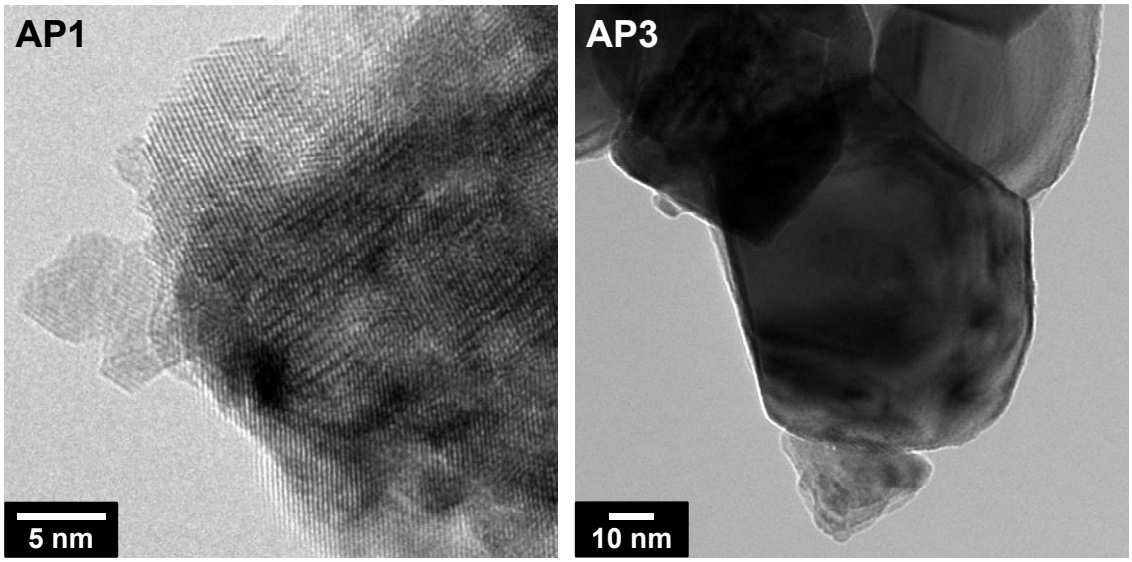

Figure 2 TEM images of Pd/CeO_2 before (AP1) and after ageing at 900 °C for 25 h in a flow of 10% H_2O/air (AP3).

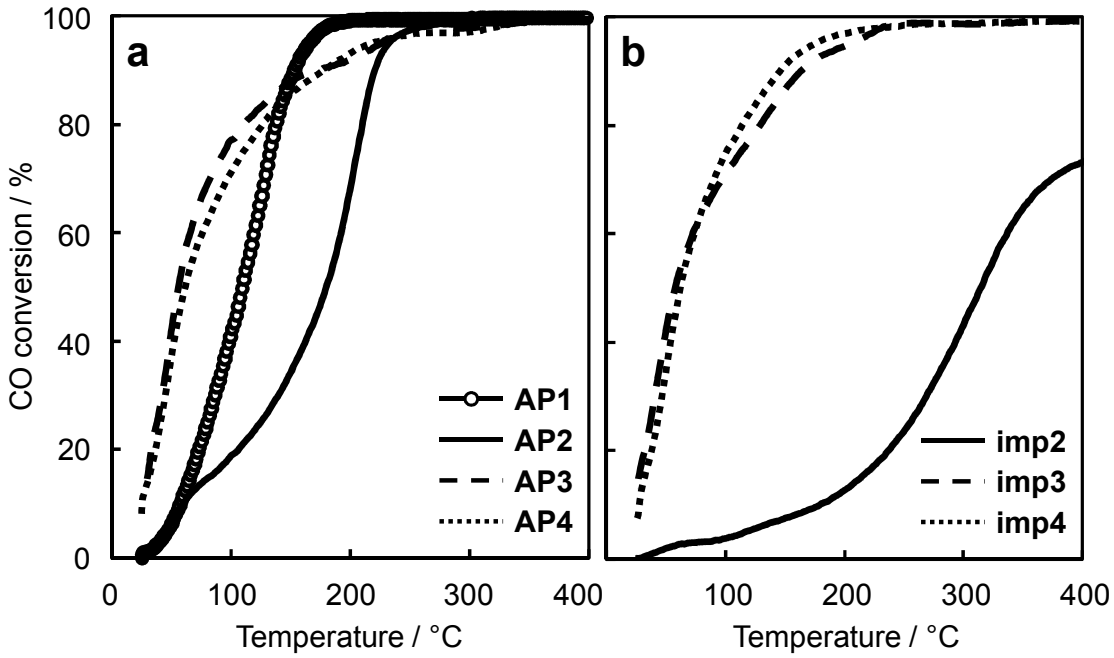

Figure 3 Temperature dependence of CO oxidation over (a) Pd/CeO_2(AP1~AP4) and (b) Pd/CeO_2(imp2~imp4) before and after thermal ageing. Reaction conditions: 0.1% CO, 1.25% O_2, He balance, W/F = 5.0×10^{-4} g·min·cm^{-3}.

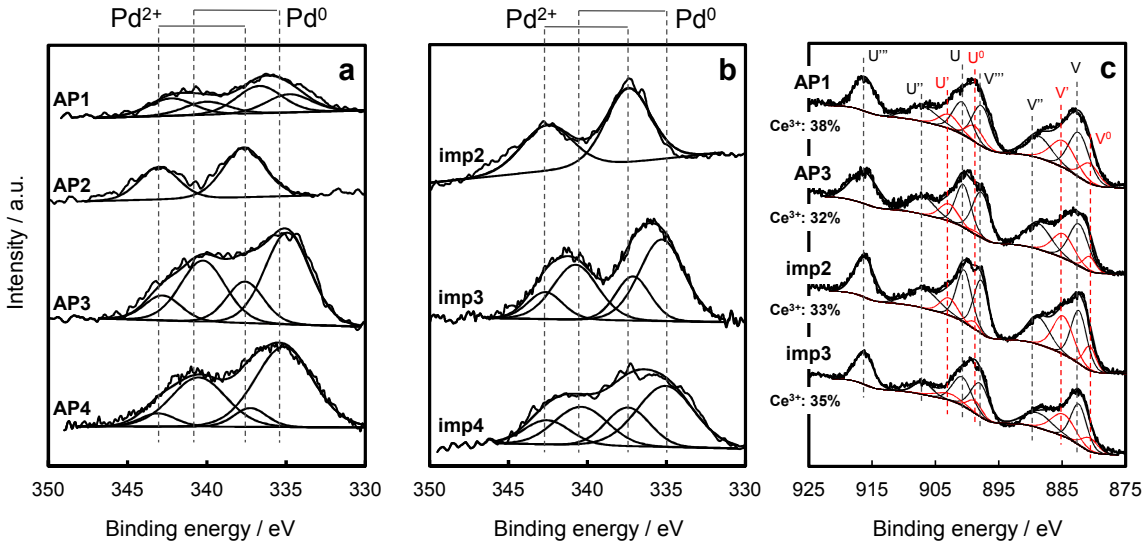

Figure 4 Pd3d XPS spectra of (a) Pd/CeO_2(AP1~AP4) and (b) Pd/CeO_2(imp2~imp4) and (c) Ce3d XPS spectra of Pd/CeO_2 (AP1, AP3, imp2 and imp3).

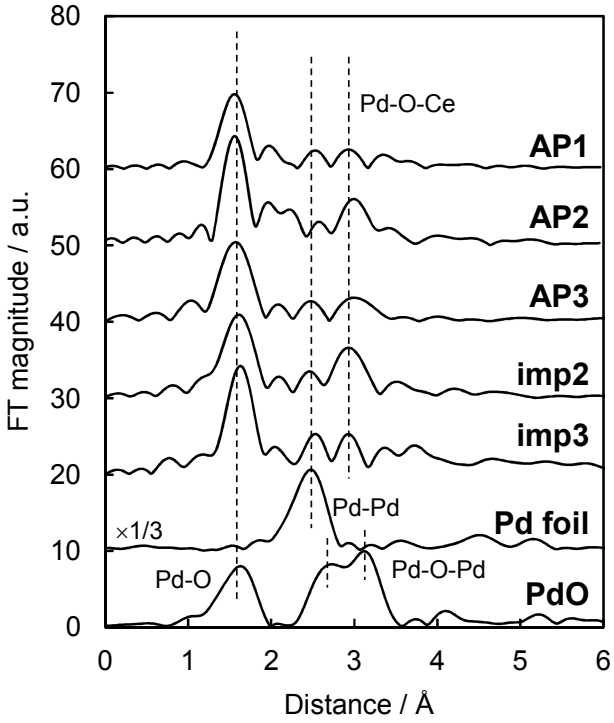

Figure 5 Fourier transforms of k^3-weighted Pd K-edge EXAFS for Pd/CeO_2(AP1~AP3) and Pd/CeO_2(imp2 and imp3) and references (PdO and Pd foil).

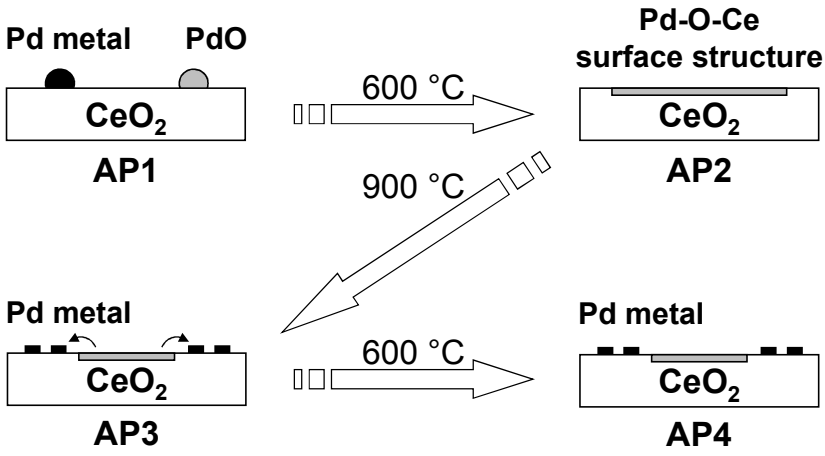

Figure 6 Possible structural changes in Pd/CeO_2(AP1~AP4) during thermal ageing.